Atmos. Chem. Phys. Discuss., 7, 10439–10465, 2007
www.atmos-chem-phys-discuss.net/7/10439/2007/

Atmospheric Chemistry and Physics Discussions

Mesoscale inversion: first results from the CERES campaign with synthetic data

T. Lauvaux[1,2], M. Uliasz[3], C. Sarrat[2], F. Chevallier[1], P. Bousquet[1], C. Lac[2], K. J. Davis[4], P. Ciais[1], A. S. Denning[3], and P. Rayner[1]

[1]Laboratoire des Sciences du Climat et de l'Environnement/IPSL,CEA-CNRS-UVSQ, Gif-sur-Yvette, France
[2]Centre Nationale des recherches Météorologiques, Toulouse, France
[3]Department of Atmospheric Sciences, Colorado State University, Fort Collins, Colorado, USA
[4]Department of Meteorology, The Pennsylvania State University, University Park, Pennsylvania, USA

Received: 25 April 2007 – Accepted: 18 July 2007 – Published: 19 July 2007

Correspondence to: T. Lauvaux (thomas.lauvaux@lsce.ipsl.fr)

Abstract

We investigate the ability of a mesoscale model to reconstruct CO_2 fluxes at regional scale. Formally, we estimate the reduction of error for a CO_2 flux inversion at 8 km resolution in the South West of France, during four days of the CarboEurope Regional Experiment (CERES) in spring 2005. Measurements from two towers and two airplanes are available for this campaign. The lagrangian particle dispersion model LPDM was coupled to the non-hydrostatic model Meso-NH and integrated in a matrix inversion framework. Impacts of aircraft and tower measurements are quantified separately and together. We find that the configuration with both towers and aircraft is able to significantly reduce uncertainties on the 4-day averaged CO_2 fluxes over about half of the 300×300 km domain. Most of this reduction comes from the tower measurements, even though the impact of aircraft measurements remains noticeable. The noise contributed by imperfect knowledge of boundary inflows does not significantly impair the resolution. We test alternative strategies to improve the impact of aircraft measurements and find that most information comes from measurements inside the boundary layer.

1 Introduction

Carbon dioxide (CO_2) has increased by 35% in the atmosphere since pre-industrial times, due to human-induced releases to the atmosphere. However, less than half % of emitted CO_2 remains in the atmosphere (Raupach et al., 2007) because continental ecosystems and oceans partly offset our emissions. The quantification of continental sources and sinks of CO_2 remains a critical step in understanding and managing the terrestrial carbon cycle. The two complementary approaches to this quantification are termed bottom-up or top-down. In the bottom-up approaches pointwise estimates of CO_2 exchange at the surface (Baldocchi et al., 2001) are integrated in space and time or are used to validate and calibrate land surface models (Krinner et al., 2005)

together with satellite retrievals of surface properties. In top-down approaches, these integrated fluxes are inferred from their signatures on atmospheric concentration after being transported in the atmosphere (Enting, 2002, Rodgers, 2000). Bottom-up methods have smallest representativity error at small scales where the demands on extrapolation are smallest, while top-down methods have been limited to large spatial scales such as continents and ocean basins (e.g. Bousquet et al., 2000, Gurney et al., 2002, Baker et al., 2007) by the difficulties of simulating atmospheric transport at smaller scales on the continents (Geels et al., 2007, Pérez-Landa et al., 2007), and also due to the sparsity of global atmospheric observations.

In this paper we demonstrate the use of a top-down approach at a regional scale of 8 km using observations from an intensive measurement campaign (Dolman et al., 2006), and atmospheric mesoscale modelling. The campaign was part of the CARBOEUROPE regional experiment (CERES). The domain of CERES is a 300 km×300 km zone, located in the south west of France (Fig. 1). We extend the domain of simulation to 720 km×720 km to investigate the complete area of influence of the measurements. With this larger domain, the boundary influence corresponds to more distant contributions depending on the global or synoptic transport. Previous attempts at downscaling top-down methods have limited themselves to larger domains (thousands of km) for carbon flux inversions (e.g. Carouge, 2006, Gerbig et al., 2003), or other trace gases as methane (Vermeulen et al., 1999). We present a demonstration system for regional inversions of CO_2 fluxes based on a mesoscale atmospheric model coupled with a lagrangian transport model. Both models are limited-domain models. We translate atmospheric observations into maps of error reduction on CO_2 fluxes over the model domain, given prior error statistics on fluxes and observations. This technique, relying on the linearity of the inversion problem, has been widely used in atmospheric inverse studies (e.g. Gloor et al., 2000, Rayner and O'Brien, 2001, Law et al., 2003). The impact of observations from continuous ground-based towers and from aircraft on the uncertainties in 1) lateral boundary conditions and 2) surface fluxes are compared. Relations between measurement altitudes (tower and aircraft)

and zones (surfaces or boundaries) influencing observations are presented and analysed. Finally, we discuss the potential of such a mesoscale inversion system to retrieve regional CO_2 fluxes.

2 Description of CERES

This mesoscale inversion takes advantage of a dense observation network which is only feasible during a short campaign over a limited domain. During CERES (Dolman et al., 2006), CO_2 concentration measurements on instrumented towers and aircraft were collected during six weeks in May–June 2005. The domain of the campaign includes the pine forest of Les Landes (West) and a large agricultural area with a mixture of winter and summer crops, in the south west of France (Figure 1), from Bordeaux (north west) to Toulouse (south east). Compared to other regional studies involving aircraft such as COBRA (CO_2 Budget and Regional Airborne Study, Stephens et al., 2000) or CAATER (Coordinated Access to Aircraft for Transnational Environmental Research, Filippi et al., 2003), the CERES domain covers a smaller region of about 300×300 km with several flights each day. Other similarly-sized domains include the "Ring of Towers" in North America (Uliasz et al., 2005) which comprises a larger set of instrumented towers but without aircraft, or RECAB (Regional Assessment and Monitoring of the Carbon Balance within Europe, Dolman et al., 2002) where aircraft were used but without towers.

CERES experiment involved two aircraft measuring atmospheric CO_2 during several Intensive Observation Periods (IOP), and two towers (Marmande and Biscarosse) measuring atmospheric CO_2 continuously (Fig. 1). Both towers provide CO_2 concentrations every 30 min, which we average hourly. The Biscarosse tower is located 2 km from the Atlantic shore, in the pine forest of Les Landes, at 50 m height on a 70-m hill. Marmande is located further inland, at 20 m height, between the pine forest and the agricultural area on the East. In this paper, we study the second IOP (26 and 27 May 2005). The two aircrafts, a Piper-Aztec and an ECO-Dimona, flew ten times between

the 23 to the 27 May during the morning and the early afternoon, with different transects in the region. We used in this study all the different flights. Some of them consist in a vertical profile above the pine forest; some others correspond to a transect from Biscarosse to Marmande, and also longer ones from Bordeaux to Toulouse mostly in the planetary boundary layer. CO_2 concentrations are measured at high frequency (1 Hz), and finally averaged to three-minute periods as detailed below.

3 Models

In order to perform a mesoscale inversion, the non-hydrostatic atmospheric mesoscale model MesoNH (Lafore et al., 1998) was coupled to the lagrangian dispersion model LPDM (Uliasz, 1994). The mesoscale model enables us to simulate atmospheric dynamics at high resolution within the domain together with high frequency CO_2 observations of the CERES campaign. The Lagrangian model is computationally efficient enough to allow the multiple backward tracer calculations required for the inversion. While the resolution of mesoscale models improves the simulation (and hence utility) of observations it comes at the cost of a limited domain size and limited duration. The two resolutions used in the two way nesting simulations of MESO-NH correspond to 8 km and 2 unitkm on the horizontal grid, with 65 levels on the vertical grid, up to 13 km altitude. The 2 km resolution simulation was used for an intensive aircraft flight time period the 27 May, and was also included in the longer simulation from the 23 to the 27 May at 8 km resolution. The 2-way nesting configuration keeps the consistency of the dynamics between the different grids, which allows us to use the particle distributions from different runs together. These two simulations use the reanalysed data from the ECMWF as initial and boundary conditions. Dynamical fields were saved each 20 minutes, or five minutes during the flights, for the off-line coupling with a lagrangian model. The dynamical fields at 2 km resolution allow a more precise description of the vertical transport during the flights. An intercomparison study between different RAMS model versions, WRF, and MesoNH, all of them coupled with biospheric models and

prescribed anthropogenic emissions, showed their ability during the CERES campaign to reproduce observed CO_2 concentrations on aircraft (Sarrat et al., 2007).

The tracer backward transport was simulated here by the Lagrangian Particle Dispersion Model (LPDM) described by Uliasz (1994). Particles are released from the receptors in a "backward in time" mode with the wind fields generated by the eulerian model MesoNH. In a "backward in time" transport mode, particles are released in LPDM from the measurement locations and travel to the surface and the boundaries. Compared to a forward mode, all the particles are used to estimate fluxes, which reduces the computational cost of the simulation. The lagrangian model LPDM was enhanced to simulate aircraft observations based on the precise trajectory of the airplane estimated by GPS (Global Positioning System). At each second, 10 particles are released at the position of the aircraft. Compared to static receptors, aircraft require a shorter period of particle integration, and a better description of the vertical motion. For a tower, particles are integrated over time depending on the frequency of the fluxes. A moving source limits the period of integration by its representativity. The spatial extension of the moving source increases with the duration of the time period of integration. At the same time, using too short periods would induce a non representative distribution given the limited number of particles released during this period. The second difficulty concerns the vertical motion in the free troposphere. Along the aircraft path, particles are released at different altitudes from a few hundred to a few thousand meters. The vertical motion influences the eventual distribution of the particles at the surface. Particles released at high altitudes are more dependent on the mean vertical wind than particles close to the surface, driven mainly by the vertical turbulent motions.

The dynamical fields in LPDM are forced by mean horizontal winds (u, v), potential temperature, and turbulent kinetic energy (TKE) from MESO-NH. At this resolution (less than 10 km), turbulent motion corresponds to the closure of the energy budget at each time step. This scalar is used to quantify turbulent motion of particles as a pseudo random velocity. Based on the TKE, wind, and potential temperature, the lagrangian model diagnoses turbulent vertical velocity and dissipation of turbulent energy. The off-

line coupling between an Eulerian and a Lagrangian model solves most of the problems of non-linearity at the mesoscale. Most of the non-linear processes resolved by the atmospheric model are attributed to a scalar representing the velocity of the particles.

At each timestep (from one to 20 s), particles move with a velocity interpolated from the dynamical fields of the MESO-NH simulation (5 or 20 min). The timestep depends on the TKE, following the discretization described in Thomson (1987). Each time a particle touches the surface, its position and release time are saved. Particles here should not be considered as individual molecules (lost when touching the surface) but as an air parcel influenced by CO_2 fluxes as it moves along the ground.

The formalism for inferring source-receptor relationships from particle distributions is described by Seibert et al. (2004). From the particle positions, we calculate an influence function by integration of the released particles over time and space at the surface and for the boundaries. At each time step, the fraction of particles (released from one receptor at one time) within some volume, gives the influence of that volume on the receptor. Finally, when a particle leaves the domain, it defines also the influence from the outer domain. The influence function is then decomposed into three different terms, corresponding to the initial concentration, the surface source contribution, and the boundary fluxes (Peylin et al., 2005).

Mesoscale inversions face the problem of modelling a limited domain with potentially high contributions from the boundary fluxes. Regional inversions at the continental scale (Gerbig et al., 2003) use large domains and long study periods to decrease the impact of the lateral boundary and initial concentrations. In our study, the time period is limited by the computational cost which forces us to deal with this initial state. Inflow and outflow contributions increase also due to the short distance from the boundaries. Concentrations at domain boundaries are defined by a grid of 1° by 1° resolution (as typically used by atmospheric general circulation models) on the horizontal and 2 levels on the vertical corresponding to the boundary layer and the free troposphere. The two levels for the boundary fluxes then appear as additional unknowns in the inverse system. Here, we use only an averaged height of the boundary layer, not changing

with time, given by the daily mean boundary layer top. This coarse description of the boundaries has the advantage of introducing fewer unknowns in the inversion, but still makes it possible to study the impact of boundaries on the different receptors. For the aircraft influence functions, different time intervals for the release of particles were tested to optimize the best time period of integration. A time interval of three minutes showed the best compromise between the signal at the surface, and the spatial extension of the corresponding receptor. Considering the velocity of the aircraft (about 150 km/h), a 3-min time window corresponds to a receptor of less than 8 km long, which is the resolution of the dynamical fields in Meso-NH.

4 Inversion

The lagrangian model backward simulations provide the matrix of influence functions (J): the sensitivity of each observation to each unknown. The size of the J matrix corresponds to the dimension of the vector of surface fluxes (90×90 grid cells corresponding to 8 km×8 km each) plus the unknown boundary concentrations divided into two levels and 5 horizontal grid cells for each side of the domain. The observations consist of 102 hourly concentration measurements from each tower plus an observation each 3 minutes from each flight. The maximum number of observations treated in this study is 8140×102×2 + 8140×2040×10. The dimension of J makes it possible to solve the inverse problem using the classical matrix solution for one averaged flux per grid cell over the four days. (e.g. Tarantola, 1987, Enting, 2002). Briefly we minimize a cost function:

$$\chi^2 = \frac{1}{2}[(\boldsymbol{s}-\boldsymbol{s}_0)^T\mathbf{C}(\boldsymbol{s}_0)^{-1}(\boldsymbol{s}-\boldsymbol{s}_0) + (\mathbf{J}\boldsymbol{s}-\boldsymbol{d})^T\mathbf{C}(\boldsymbol{d})^{-1}(\mathbf{J}\boldsymbol{s}-\boldsymbol{d})] \quad (1)$$

Where $\boldsymbol{s}$ represents the unknown sources we seek, $\boldsymbol{s}_0$ the a priori source estimate, $\boldsymbol{d}$ the observed data and $\mathbf{C}(\boldsymbol{x})$ the uncertainty covariance of a vector quantity. $\mathbf{J}$ rep-

resents the Jacobian or matrix of influence functions relating sources to observations. $\boldsymbol{s}$ and $\mathbf{J}$ include concentrations at the boundary as described above. Minimizing the equation with respect to $\boldsymbol{s}$

$$\boldsymbol{s} = \boldsymbol{s}_0 + \mathbf{C}(\boldsymbol{S}_0)\mathbf{J}^T \left(\mathbf{J}\mathbf{C}(\boldsymbol{s}_0)\mathbf{J}^T + \mathbf{C}(\boldsymbol{d})\right)^{-1} (\boldsymbol{d} - \mathbf{J}\boldsymbol{s}_0) \quad (2)$$

More important for this work is the posterior error covariance for sources given by the expression:

$$\mathbf{C}(\boldsymbol{s})^{-1} = \mathbf{C}(\boldsymbol{s}_0)^{-1} + \mathbf{J}^T\mathbf{C}(\boldsymbol{d})^{-1}\mathbf{J} \quad (3)$$

We do not solve $\boldsymbol{s}$ in this paper, but focus on the uncertainties of $\boldsymbol{s}$ ($\mathbf{C}(\boldsymbol{s})$) that do not depend on the observations $\boldsymbol{d}$ but only on their errors $\mathbf{C}(\boldsymbol{d})$ and a prior error covariance $\mathbf{C}(\boldsymbol{s}_0)$. We notice in equation (3) that the posterior covariance $\mathbf{C}(\boldsymbol{s})$ depends on the prior covariance $\mathbf{C}(\boldsymbol{s}_0)$. This dependence will be discussed for our inversion by doubling the prior uncertainty for the lateral boundaries, to estimate the impact on the error reduction for the surface and the boundaries. The value of the prior flux error was set to $2\,\mathrm{gm}^{-2}\,\mathrm{day}^{-1}$ for the surface and 4 ppm for the boundaries. Concerning the estimation of the observation uncertainty, we assessed it by the comparison of the model results with aircraft data. The highest difference is about 3 ppm, on different flights of the 27 May. Taking into account the uncertainty of the LPDM model, and the lack of temporal correlations, we set the observation error at 4 ppm. Finally, we define the error reduction as:

$$\boldsymbol{r} = \frac{\boldsymbol{\sigma}_{\mathrm{post}}}{\boldsymbol{\sigma}_{\mathrm{prior}}} \quad (4)$$

where $\boldsymbol{\sigma}(\boldsymbol{x})$ is the square root of the diagonal of $\mathbf{C}(\boldsymbol{x})$. σ_{post} represents the posterior error, and σ_{prior} the prior error. Theoretically, retrieving fluxes over a 4-day period implies that the error covariance matrix on the fluxes is correlated in time. From the study of Chevallier et al. (2006) based on daily CO_2 fluxes simulated by a biosphere model and CO_2 flux observations, the time correlation of the differences between modelled

and observed CO_2 fluxes is still more than 0.5 after 5 days. Our assumption of a full error correlation over four days seems realistic even at the time correlation of CO_2 flux covariance error. Concerning the spatial correlation of the prior error covariance, we assumed uncorrelated flux errors on the domain, as the weakest constraint for this inversion. Using a spatial error correlation would lead to assume spatial coherences in CO_2 flux errors which were not clearly identified at this scale.

5 Experiments

We conducted three experiments with the inverse system. For each of them we optimized only one mean flux for the four days of measurements and for each model pixel at 8km resolution. In the first experiment, we tested the potential of the observations performed during the CERES campaign to reduce uncertainties on CO_2 fluxes. This study produces maps of error reduction over the domain. The error reduction was mapped to a final resolution at 8 km. The different receptors are simulated separately during the period. Biscarosse, Marmande, and three different flights of the 27th of May were combined to estimate the final potential of the method.

The second experiment aimed at optimizing the flight paths of the next CERES campaign planned for April and September 2007. Thus, we tested different altitudes of virtual flights in the boundary layer and tried to infer an optimal height from the diagnostic of particle distribution and from the spatial extension of the influence function. Based on one flight from the 2005 CERES campaign, we created 12 virtual flights with constant altitudes from 100 to 2500 m. The horizontal coordinates used for these virtual flights correspond to a long transect from Bordeaux to Toulouse. This optimization gives a first constraint on aircraft measurement strategy and on the dependency of spatial extension of the fluxes influencing the observations to flight altitudes .

In a third experiment, the impact of the altitude of CO_2 measurement towers was investigated. The sampling altitude of near-ground stations continuously measuring CO_2 largely determines the spatial extension of the area influencing measurements. Tall

towers observe CO_2 concentrations in the mixed layer and are able to provide information coming from larger areas (Davis et al., 2003, Gloor et al., 2001). We modelled here a virtual tall tower of 300 m height at the exact position of the actual Biscarosse tower (real altitude is 50 m). The spatial variation of the surface flux contribution is then compared to the actual one over the 4-day period.

6 Results

During this 4-day period, different meteorological situations drive the transport of particles, with mean winds in the valleys or to the Atlantic Ocean. During the 26 May, as for the 27, a sea breeze starts around noon, affecting the Biscarosse tower (Fig. 2 (b)). This situation appears on the 27th whereas the Autan wind was dominating the two towers (Fig. 2a), i.e. a strong south eastern wind amplified by the valley between the Corbieres mountains and the Montagne Noire. During the night, northen wind prevails at the Biscarosse tower, parallel to the sea shore. At the Marmande tower, even though the main wind direction remains South East, the plume of particles during the 26 May show a wave distribution corresponding to changes of the wind direction. Figure 2 shows the dominating boundary influence from the West of the domain for the beginning of the 4-day period. The dominant location changes during the other days, but remains localised, which justifies the fine description of boundary conditions. Considering the particles released from Biscarosse, we estimated the time distribution of the particles reaching the boundaries during the 27 May (Fig. 3). We chose an interval of 400 s, corresponding to 200 particles released. 15 h after their release, 99% of them left the domain. This result sets the maximum time integration required because flux increments only depend on observations in this temporal window. The synoptic winds were weak during this day (about 3 m/s), which makes this estimation an upper limit for the other days.

For the first experiment, we ran an inversion using only the two towers, measuring throughout the 4-day period (Fig. 4b). In the vicinity of the towers (tens of km), error re-

duction can reach 90% but decreases rapidly to 50%. In the directions of the main daily winds, the reduction is about 30% 300 km from the towers, in a narrow band. On the boundaries, the reduction of error is less than 1% and almost uniform on different sides of the domain. When using only the flight from Biscarosse to Marmande (Fig. 4a), the largest error reductions (about 90%) occur for one or two boundary pixels (100 km per pixel) of the upper western boundary. South of the trajectory, error reduction is about 5% in a small region of few tens of km. Another region at the East of the Pyrenees, also visible in the tower case, shows a reduction of about 1%. The last inversion uses all the different available measurements during the second CERES IOP (Fig. 4c). It shows an extended error reduction around the towers from 60 to 90%, but also some regions of larger error reduction in the East and South of the Pyrenees of 10 to 60%. As in the aircraft case, a few grid cells of the upper boundary show a reduction of about 90%, the rest being less than 10%. The error reduction at the surface is extended by the different flights, and increased by 15 to 20%. Even though one flight shows limited impact (Fig. 4b), the addition of the ten different flights is noticeable in the final error reduction.

The second experiment arises from the first one, where it appears that the surface flux contribution to CO_2 concentration measured by aircraft is reduced compared with tower observations. In order to optimize this contribution, a series of 12 virtual flights was simulated at different altitudes, from 100 m to 2500 m. Three different diagnostics were used to estimate the impact of the height of the trajectory on the surface contribution (Fig. 5) : the number of grid cells with a number of particles corresponding to an error reduction greater than 1%, to the highest reductions of error of each flight, and corresponding to the averaged error reduction for all the surface grid cells for each flight. The three different measures are constant in the boundary layer, and decrease quickly above it, with almost the same shape. Between 500 m to 1000 m, the three measures of error reduction vary due to a change in the horizontal mean wind. A local horizontal wind shear affects the particle distribution when the simulated aircraft flies in one of the main horizontal winds.

The last experiment uses only the Biscarosse tower. The two towers used for this campaign had almost the same height (20 m and 70 m). Thanks to the high resolution of the transport model, we estimated the area of influence in the case of a tall tower. A virtual "Biscarosse" tower of 300 m was simulated to estimate the height dependence, as for the aircraft. Figure 6a shows the particle "touchdowns" for the real Biscarosse tower (70 m above sea level, and 35 m above the ground). The most important region of influence covers a large area between Biscarosse and Marmande towers, and also 2 thin bands due to sea breezes of different days of the experiment. A smaller area at the East of the Pyrenees can be noticed, as with error reduction of the previous cases. Using the virtual tall Biscarosse tower, the spatial extension of surface influence is globally reduced (Fig. 6b), especially in the zone of interest around the tower, and elsewhere not visibly enhanced. Concerning the boundaries, reduction remains equivalent, reduced to less than 1%. The night time signal is mainly responsible for the weaker surface response obtained with a virtual tall tower. This is a case where our choice to solve for night and day fluxes together has a significant impact.

7 Discussion

For the second CERES IOP, estimated error reduction larger than 30% covers an area of about 200 km in the North-South direction and 100 km in the West-East direction. This allows optimizing surface fluxes with a real inversion in the zone of interest, corresponding to the pine tree forest and part of the agricultural area. Aircraft data showed a small but noticeable contribution at the surface although the time of integration is limited to a few minutes during a flight of a few hours. One needs to recall two aspects of the inverse set-up when weighing this contribution. Firstly we assumed that flux increments were invariant over four days. From the viewpoint of estimating fluxes themselves it is a crude assumption, but when considering error reduction it is equivalent to assume one can build a flux model to estimate mean fluxes over four days. Zupanski et al. (2007) made a similar assumption for 10 day periods for the ring of tow-

ers built in North America. If this assumption is relaxed, the impact of measurements and consequently the error reduction will be reduced. On the spatial side, we made no assumption about the spatial smoothness of fluxes. This is consistent with the recent results of Chevallier et al. (2006) but not with the introduction of spatially decaying error correlation in large-scale inverse studies (Rödenbeck et al., 2003; Peylin et al., 2005). The addition of spatial error correlations decreases the effective number of unknowns and hence increases the impact of measurements. But, at the resolution of a few kilometers, more work is necessary on the topic of correlation, both in space and in time. The inverse system we set up can handle such correlations.

In our inverse system, boundaries appear to be only weakly constrained by observations compared to surface fluxes. The final contribution of boundaries remains limited because particles released in LPDM touch the surface three times on average before leaving the domain after passing once through the boundaries. For tower data, boundary conditions have a reduced contribution on the observed concentrations at this scale. For aircraft, the contribution of the boundaries is more important due to the fact that most of the particles released at higher altitudes reach the boundaries without touching the surface. However, even with the use of aircraft, the optimization of the boundary fluxes remains limited because aircraft measurements represent many fewer particles than continuous ground sites. This means also that the impact of the boundaries on final CO_2 concentrations observed is reduced. Most of the influence during mesoscale processes can be attributed to the near surface measurements. The prior uncertainty of the boundaries was increased to assess its impact on the posterior error. As a result, the error reduction remains constant whereas high values at the boundaries show higher reductions. First, the result is explained by Eq. (3). For a given $\mathbf{C}(\boldsymbol{d})$ and $\mathbf{J}$ there is a larger reduction of error if $\mathbf{C}(\boldsymbol{s}_0)^{-1}$ is small, i.e. a large prior uncertainty. The lack of impact on the reduction of error for the surface is explained by the weak coupling between the surface and boundary parts of the inversion. Another solution to optimize boundary fluxes could also consist in adding an offset concentration in the inverse system, with an uncertainty, large enough to compensate for large scale model

errors.

Overall, for short term mesoscale inversions, the need for constraint at the boundaries is clear for high altitude observations, but not in the boundary layer. Global models seem to be able to give this information at least in the context of weak mean wind and strong convection near the surface. The use of global models to constrain boundaries might also be critical when using tall towers. As shown by the third experiment, such towers are mainly influenced by large scale motions.

The high spatial resolution used for this inversion shows that the most observable flux contribution comes from regions close to the measuring instruments within the boundary layer. This spatial distribution is strongly dependent on the quality of atmospheric transport, but mesoscale models like MesoNH have shown their ability to reproduce complex dynamical processes in the lower atmosphere (Sarrat et al., 2007). Compared to larger scale inversions, mesoscale inversions have the potential to solve higher temporal and spatial resolution fluxes but on a reduced area. In this context, the comparison with previous methods remains difficult looking at the spatial extension of the analysis.

High resolution inversions could be used to improve on large scale inversions thanks to reduced transport and representativity errors. Compared to the 1° by 1° resolution grid used in advanced global inversions, the actual meso scale inversion could optimize fluxes over 2 grid cells of the large scale model, without any spatial correlation in the prior uncertainty. This footprint, although not large, is much greater than that of the flux towers traditionally used in bottom-up inversions. Mesoscale inversions seem to be able to optimize surface fluxes of carbon for different land covers or, following the data assimilation approaches of Rayner et al. (2005), vegetation parameters. This application could improve vegetation model parameterization of the carbon cycle and closely-coupled water cycle.

For the 27 May, the high surface temperatures observed (35 degrees Celsius at 02:00 p.m.) contribute to a fast mixing of the whole convective boundary layer (CBL). During the day time (boundary layer height reaches 2000 m at its maximum thickness).

Averaged vertical velocity estimated in a preliminary simulation appeared to be weaker than observed. A simple first approach to examining the importance of this issue is to estimate the impact of strongly varying day/night turbulence intensities and depth of mixing. This can be approximated with vertical turbulent velocities of a few meters per second and mixing depths of one to two kilometers for a strongly convective diurnal boundary layer such as 27 May. The present LPDM parameterization for boundary layer turbulence corresponds to Gaussian but inhomogeneous conditions (Thomson, 1987, Du, 1997). Using enhanced mixing in a test, we found that error reduction was smaller due to a loss of particles to the free troposphere. A more sophisticated planetary boundary layer scheme should be developed to improve the vertical mixing in LPDM. This development needs the description of other dynamic processes such as entrainment and detrainment at the top of the planetary boundary layer. We will investigate such a scheme in the context of an inversion using actual measurements.

Finally, towers are the most important source of information for the inversion of surface fluxes. At the same time, aircraft allow us to constrain the limits with only a small effect on the final surface fluxes and their posterior uncertainties. The combination of these observations defines a complete framework to assess sources and sinks for mesoscale domains.

8 Conclusions

We have developed here a demonstrator for regional inverse modelling at the meso scale, and tested it for the CERES intensive campaign (2nd IOP). Using available measurement locations and dates, a large part (more than 50%) of the domain (300 km×300 km) is constrained with an error reduction larger than 30%. No spatial a priori correlation was used to enlarge the impact of the data. Concentration measurements on towers play a major role in reducing uncertainties for surface fluxes, whereas aircraft measurements above the planetary boundary layer influence mostly the boundaries. The intensive period of flights improved the error reduction at the surface by 15 to

20% compared with the two tower-only case. This implies also a reduced importance of boundary conditions compared to surface influence for near ground observations, in the larger domain of the nesting configuration (700 km×700 km).

Acknowledgements. We wish to thank all participants in the CERES campaign for making their data freely available. CarboEurope is supported by the European Commission under the 6th Framework Programme.

References

Baker, D. F., Law, R. M., Gurney, K. R., Rayner, P., Peylin, P., Denning, A. S., Bousquet, P., Bruhwiler, L., Chen, Y.-H., Ciais, P., Fung, I. Y., Heimann, M., John, J., Maki, T., Maksyutov, S., Masarie, K., Prather, M., Pak, B., Taguchi, S., and Zhu, Z.: TransCom 3 inversion intercomparison: Impact of transport model errors on the interannual variability of regional CO2 fluxes, 1988–2003, Global Biogeochem. Cycles, 20, GB1002, doi:10.1029/2004GB002439, 2007. 10441

Baldocchi, D. D., Falge, E., Gu, L., Olson, R., Hollinger, D., Running, S., Anthoni, P., Bernhofer, C., Davis, K., Fuentes, J., Goldstein, A., Katul, G., Law, B., Lee, X., Malhi, Y., Meyers, T., Munger, J. W., Oechel, W., Pilegaard, K., Schmid, H. P., Valentini, R., Verma, S., Vesala, T., Wilson, K., and Wofsy, S.: FLUXNET: A new tool to study the temporal and spatial variability of ecosystem-scale carbon dioxide, water vapor, and energy flux densities, Bull. Am. Meteorol. Soc., 82, 2415–2435, 2001. 10440

Bousquet, P., Peylin, P., Ciais, P., Quéré, C. L., Friedlingstein, P., and Tans, P. P.: Regional changes in carbon dioxide fluxes of land and oceans since 1980, Science, 290, 1342–1346, 2000. 10441

Carouge, C.: Vers une estimation des flux de CO_2 Européen, PhD thesis, 2006. 10441

Chevallier, F., Viovy, N., Reichstein, M., and Ciais, P.: On the assignment of prior errors in Bayesian inversions of CO_2 surface fluxes, Geophys. Res. Lett., 33, L13802, doi:10.1029/2006GL026496, 2006. 10447, 10452

Davis, K., Bakwin, P., Berger, B., Yi, C., Zhao, C., Teclaw, R., and Isebrands, J.: The annual cycle of CO2 and H2O exchange over a northern mixed forest as observed from a very tall tower, Global Change Biology, 9, 1278–1293, 2003. 10449

Dolman, A. J., Noilhan, J., Durand, P., Sarrat, C., Brut, A., Piguet, B., Butet, A., Jarosz, N., Brunet, Y., Loustau, D., Lamaud, E., Tolk, L., Miglietta, R. R. F., Gioli, B., Magliulo, V., Esposito, M., Gerbig, C., Krner, S., Galdemard, P., Ramonet, M., Ciais, P., Neininger, B., Hutjes, R. W. A., Macatangay, J. A. E. R., Schrems, O., Pérez-Landa, G., Sanz, M. J., Scholz, Y., Facon, G., Ceschia, E., and Beziat, P.: CERES, the CarboEurope Regional Experiment Strategy in Les Landes, South West France, May-June 2005, Bull. Am. Meteorol. Soc., doi:10.1175/BAMS–87–10–1367, 2006. 10441, 10442

Dolman, H., DeMartino, B., Gioli, B., Hutjes, R. W. A., Lindroth, A., Miglietta, F., Millan, M. M., Sanz, M. J., and Schumacher, M.: Regional assessment and monitoring of the carbon balance within Europe (RECAB): Experimental strategy and mesoscale modeling preliminary results, European Geophysical Union, Nice, EGS02-A-06856, 2002. 10442

Du, S.: Universality of the lagrangian velocity structure function constant (C0) across different kinds of turbulence, Bound. Lay. Meteorol., 83, 207–219, 1997. 10454

Enting, I. G.: Inverse Problems in Atmospheric Constituent Transport, Cambridge University Press, 2002. 10441, 10446

Enting, I. G., Trudinger, C. M., and Francey, R. J.: A synthesis inversion of the concentration and $\delta^{13}C$ of atmospheric CO_2, Tellus, 47B, 35–52, 1995.

Filippi, D., Ramonet, M., Ciais, P., Picard, D., Roulley, J.-C. L., Schmidt, M., and Nedelec, P.: Greenhouse airborne measurements over Europe, Geophys. Res. Abstracts, 5, 2003. 10442

Geels, C., Gloor, M., Ciais, P., Bousquet, P., Peylin, P., Vermeulen, A. T., Dargaville, R., Aalto, T., Brandt, J., Christensen, J., Frohn, L. M., Haszpra, L., Karstens, U., Rödenbeck, C., Ramonet, M., Carboni, G., and Santaguida, R.: Comparing atmospheric transport models for future regional inversions over Europe. Part 1: Mapping the CO2 atmospheric signals, Atmos. Chem. Phys., 7, 3461–3479, 2007, http://www.atmos-chem-phys.net/7/3461/2007/. 10441

Gerbig, C., Lin, J. C., Wofsy, S. C., Daube, B. C., Andrews, A. E., Stephens, B. B., Bakwin, P. S., and Grainger, C. A.: Toward constraining regional-scale fluxes of CO_2 with atmospheric observations over a continent: 2. Analysis of COBRA data using a receptor-oriented framework, J. Geophys. Res., 108(D24), 4757, doi:10.1029/2003JD003770, 2003. 10441, 10445

Gloor, M., Fan, S. M., Pacala, S., and Sarmiento, J.: Optimal sampling of the atmosphere for purpose of inverse modeling: A model study, Global Biogeochem. Cycles, 14, 407–428, 2000. 10441

Gloor, M., Bakwin, P., Hurst, D., Lock, L., Draxler, R., and Tans, P.: What is the concentration

footprint of a tall tower?, J. Geophys. Res., 106, 17 831–17 840, 2001. 10449
Gurney, K. R., Law, R. M., Denning, A. S., Rayner, P. J., Baker, D., Bousquet, P., Bruhwiler, L., Chen, Y.-H., Ciais, P., Fan, S., Fung, I. Y., Gloor, M., Heimann, M., Higuchi, K., John, J., Maki, T., Maksyutov, S., Masarie, K., Peylin, P., Prather, M., Pak, B. C., Randerson, J., Sarmiento, J., Taguchi, S., Takahashi, T., and Yuen, C.-W.: Towards robust regional estimates of CO_2 sources and sinks using atmospheric transport models, Nature, 415, 626–630, 2002. 10441
Krinner, G., Viovy, N., de Noblet-Ducoudré, N., Ogee, J., Polcher, J., Friedlingstein, P., Ciais, P., Sitch, S., and Prentice, I. C.: A dynamic global vegetation model for studies of the coupled atmosphere-biosphere system, Global Biogeochem. Cycles, 19, GB1015, doi:10.1029/2003GB002199, 2005. 10440
Lafore, J., Stein, J., Bougeault, P., Ducrocq, V., Duron, J., Fischer, C., Hereil, P., Mascart, P., Masson, V., Pinty, J. P., Redelsperger, J., Richard, E., and de Arellano, J. V.: The Meso-NH atmospheric simulation system. Part I: adiabatic formulation and control simulations, Ann. Geophys., 16, 90–109, 1998, http://www.ann-geophys.net/16/90/1998/. 10443
Law, R. M., Rayner, P. J., Steele, L. P., and Enting, I. G.: Data and modelling requirements for CO_2 inversions using high frequency data, Tellus, 55B, 512–521, doi:10.1034/j.1600-0560.2003.0029.x, 2003. 10441
Pérez-Landa, G., Ciais, P., Gangoiti, G., Palau, J. L., Carrara, A., Gioli, B., Miglietta, F., Schumacher, M., Millan, M. M., and Sanz, M. J.: Mesoscale circulations over complex terrain in the Valencia coastal region, Spain, Part 2: linking CO_2 surface fluxes with observed concentrations, Atmos. Chem. Phys., 7, 1851–1868, 2007, http://www.atmos-chem-phys.net/7/1851/2007/. 10441
Peylin, P., Rayner, P. J., Bousquet, P., Carouge, C., Hourdin, F., Ciais, P., Heinrich, P., and AeroCarb Contributors: Daily CO_2 flux estimate over Europe from continuous atmospheric measurements: Part 1 inverse methodology, Atmos. Chem. Phys., 5, 3173–3186, 2005, http://www.atmos-chem-phys.net/5/3173/2005/. 10445, 10452
Raupach, M. R., Marland, G., Ciais, P., Le Quere, C., Canadell, J. G., Klepper, G., and Field, C. B.: Global and regional drivers of accelerating CO2 emissions, PNAS, 104, 10 288–10 293, http://www.pnas.org/cgi/content/abstract/104/24/10288, 2007. 10440
Rayner, P. J. and O'Brien, D. M.: The utility of remotely sensed CO_2 concentration data in surface source inversions, Geophys. Res. Let., 28, 175–178, 2001. 10441
Rayner, P. J., Scholze, M., Knorr, W., Kaminski, T., Giering, R., and Widmann, H.:Two decades

of terrestrial Carbon fluxes from a Carbon Cycle Data Assimilation System (CCDAS), Glob. Biogeochem. Cyc., 19, 2026, doi:10.1029/2004GB002254, 2005. 10453
Rödenbeck, C., Houweling, S., Gloor, M., and Heimann, M.: Time-dependent atmospheric CO_2 inversions based on interannually varying tracer transport, Tellus B, 55, 488–497, 2003. 10452
Rodgers, C. D.: Inverse methods for atmospheric sounding: Theory and practice, World Scientific Publishing Co. Pte. Ltd. 2000. 10441
Sarrat, C., Noilhan, J., Lacarrère, P., Donier, S., Dolman, H., Gerbig, C., Ciais, P., and Butet, A.: Atmospheric CO_2 modeling at the regional scale: Application to the CarboEurope Regional Experiment, J. Geophys. Res., 112, D12105, doi:10.1029/2006JD008107, 2007. 10453
Sarrat, C., Noilhan, J., Dolman, H., Gerbig, C., Ahmadov, R., Tolk, L. F., Meesters, A. G. C. A., Hutjes, R. W. A., Ter Maat, H. W., Pérez-Landa, G., Donier, S.: Atmospheric CO_2 modeling at the regional scale: an intercomparison of 5 meso-scale atmospheric models, Biogeosciences Discuss., 4, 1923–1952, 2007, http://www.biogeosciences-discuss.net/4/1923/2007/. 10444
Seibert, P., Frank, A.: Source-receptor matrix calculation with a Lagrangian particle dispersion model in backward mode, Atmos. Chem. Phys., 4, 51–63, 2004 10445
Stephens, B. B., Wofsy, S. C., Keeling, R. F., Tans, P., and Potosnak, M. J.: The CO_2 Budget and Rectification Airborne Study: Strategies for measuring rectifiers and regional fluxes, Inverse Methods in Global Biogeochemical Cycles, Geophysical Monograph 114, AGU, 2000. 10442
Tarantola, A.: Inverse Problem Theory: Methods for Data Fitting and Parameter Estimation, Elsevier, Amsterdam, 1987. 10446
Thomson, D. J.: Criteria for the selection of stochastic models of particle trajectories in turbulent flow, J. Fluid Mech., 180, 529–556, 1987. 10445, 10454
Uliasz, M.: Lagrangian particle modeling in mesoscale applications, Environmental Modelling II, ed. P. Zanetti, Computational Mechanics Publications, 71–102, 1994. 10443, 10444
Uliasz, M., Denning, A. S., Schuh, A., Richardson, S. J., Miles, N., Davis, K. J., and Zupanski, D.: Estimation of regional CO2 fluxes using concentration measurements from the ring of towers in northern Wisconsin, American Geophysical Union, Fall Meeting, 2005. 10442
Vermeulen, A. T., Eisma, R., Hensen, A., and Slanina, J.: Transport model calculations of NW-European methane emissions, Env. Sci. and Policy, 2, 315–324, 1999. 10441
Zupanski, D., Denning, A. S., Uliasz, M., Zupanski, M., Schuh, A. E., Rayner, P. J., Peters, W., and Corbin, K.: Carbon flux bias estimation employing Maximum Likelihood Ensemble Filter

(MLEF), J. Geophys. Res., in press, 2007. 10451

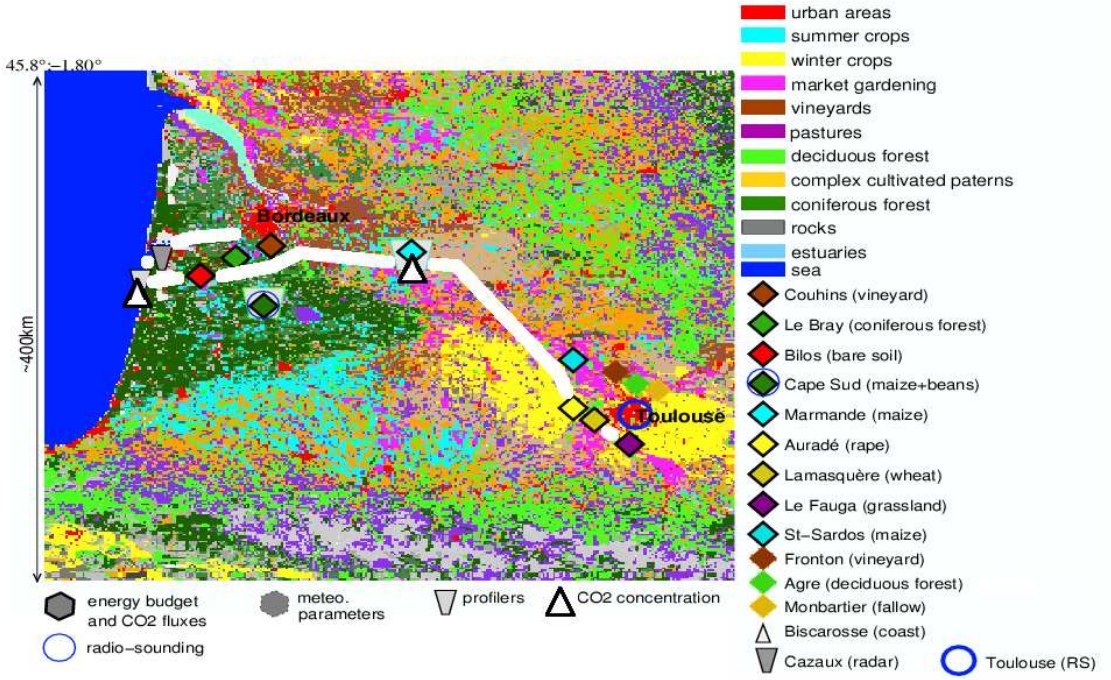

Fig. 1. Map of the vegetation types and the instrumentation over the CERES domain for the campaign 2005.

ACPD
7, 10439–10465, 2007

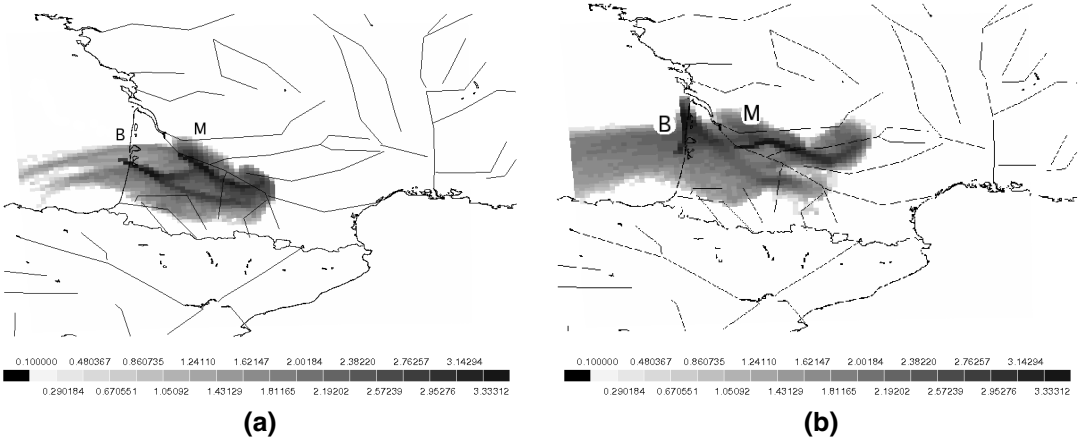

Fig. 2. Distribution of the particles (logarithmic scale) released from Biscarosse (B) and Marmande (M) towers **(a)** the 27 May between 06:30 a.m. and 07:30 a.m. **(b)** the 26 May between 08:30 p.m. and 09:30 p.m.

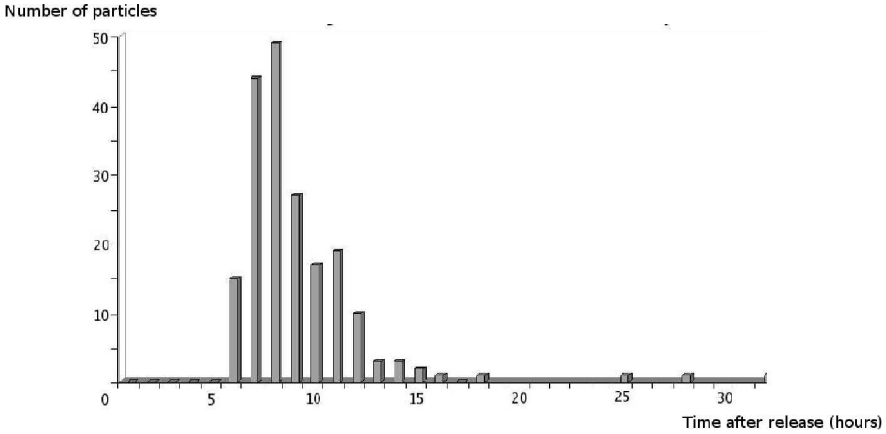

Fig. 3. Time distribution of the particles leaving the domain, released in a 400-s interval (equivalent to 200 particles) at Biscarosse tower.

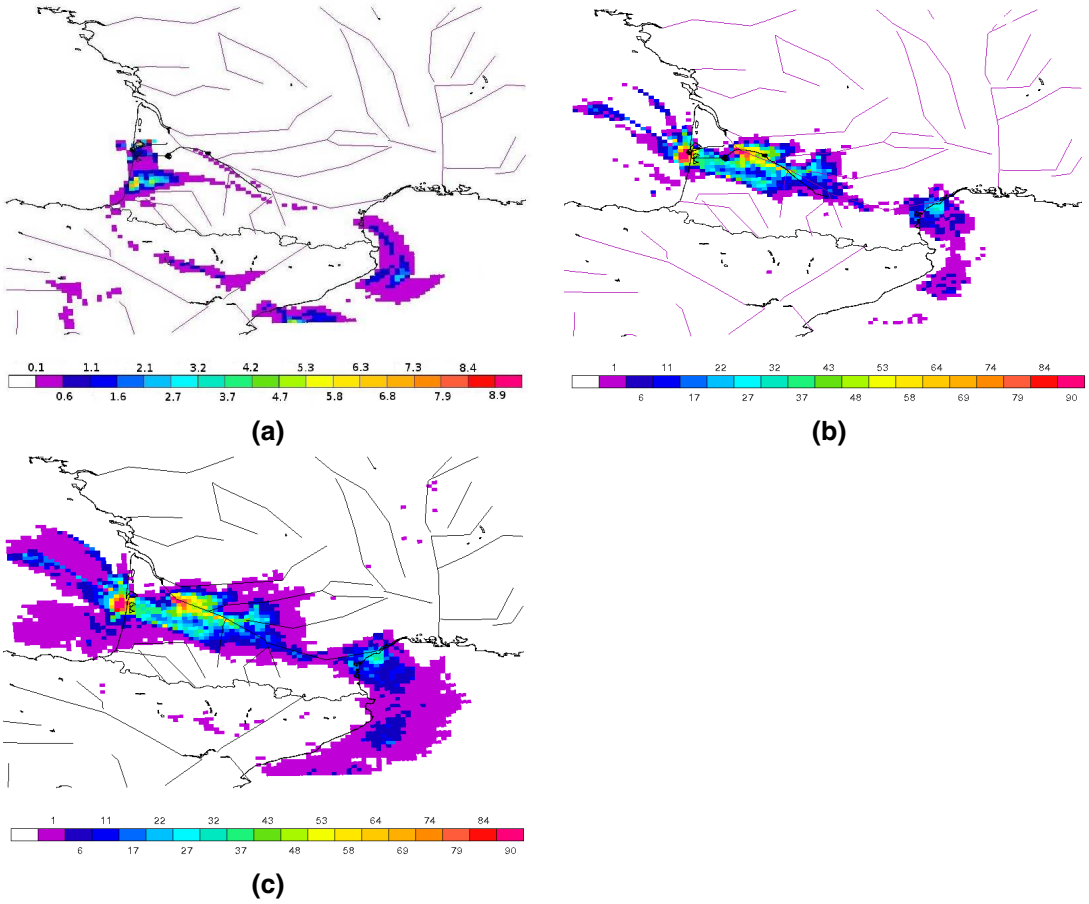

Fig. 4. Error reduction (%) on surface fluxes over the 4-day period: **(a)** Piper Aztec flight **(b)** 2 towers, **(c)** 2 towers + 10 flights.

ACPD
7, 10439–10465, 2007

EGU

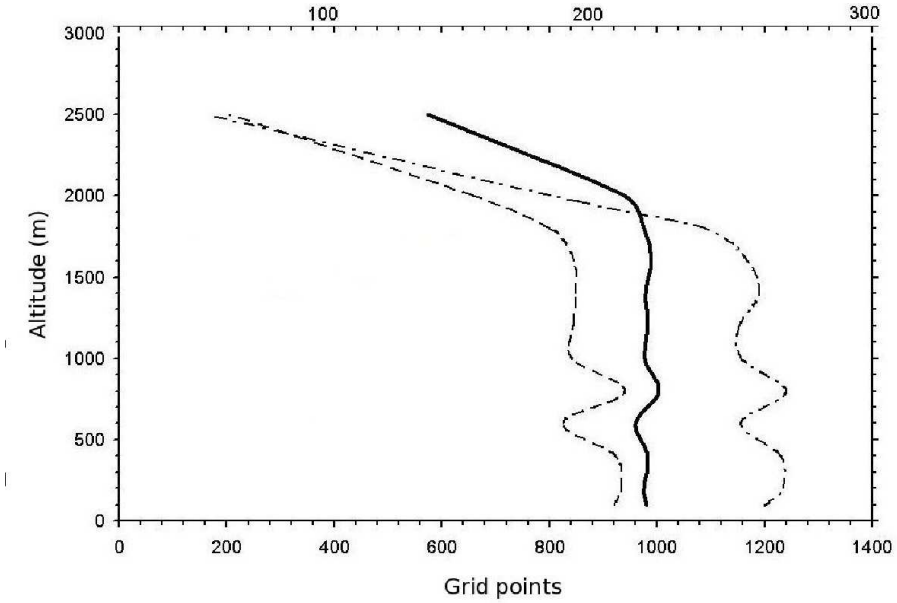

Fig. 5. Number of grid cells with an error reduction of 1% (solid line), with an error reduction equals or more than 30% (dashed line, top x-axis) and the averaged value of the error reduction within the domain (dash-dotted line) depending on the altitude of the virtual flights.

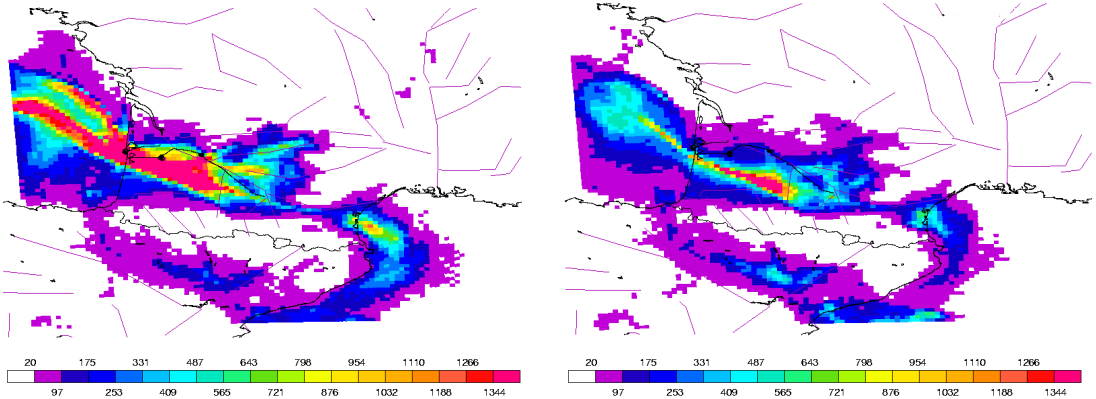

Fig. 6. Particle distribution over 4-day period: **(a)** Real Biscarosse tower (70 m), **(b)** Fictive tall tower at Biscarosse (300 m).